RSC Advances

A Novel in situ Self Foaming Method for the Synthesis of Porous Calcium Metaphosphate Biomaterials

Journal:	*RSC Advances*
Manuscript ID:	RA-ART-09-2014-011097.R1
Article Type:	Paper
Date Submitted by the Author:	02-Nov-2014
Complete List of Authors:	zhang, yin; Nanjing Tech University, Yao, Nengjian; Nanjing Tech University, Li, Wenhui; Nanjing Tech University, jiang, shengxiang; Nanjing Tech University, wang, fei; Nanjing Tech University,

Correspondence should be addressed to Yin Zhang at the following address, phone and fax number, and email address:

Address: NO.5 Xinmofan Road, Nanjing, 210009, China

Nanjing Tech University,

E-mail: zhang.512@njtech.edu.cn

Tel: 00862583587260

Fax: 00862583587260

A Novel in situ Self Foaming Method for the Synthesis of Porous Calcium Metaphosphate Biomaterials

Yin Zhang[*,1,2], Nengjian Yao[1], Fei Wang[1], Wenda Li[1] and Shengxiang Jiang[1]

[1]College of Materials Science and Engineering, Nanjing Tech University, Nanjing 210009, China

[2]Nanjing Haoqi Advanced Materials Co., Ltd., Nanjing, 211300, China

Abstract

Porous calcium metaphosphate (CMP) ceramics were manufactured using an in situ self-foaming method. The porous CMP ceramics with different porosities and strengths, and the preparation process and the properties of resulting material were studied. Under the conditions of low molding pressure (≦2.0 MPa) or low heating rate (≦0.5 ˚C/min), green specimens synthesized using only $Ca(H_2PO_4)_2·H_2O$ (MCPM) or $Ca(H_2PO_4)_2$ (MCPA) as raw materials can be fabricated into porous bioceramics without deformation and without pore-forming agents. In this study, MCPA specimens were molded at a pressure of 80.0 MPa and the heating rate was controlled at 0.5 ˚C/min. The synthetic biomaterial showed a porosity of 38.0% and a strength of 48.0 MPa.

Keywords: Calcium metaphosphate; In situ self-foaming; Porous ceramics

1. Introduction

Tissue engineering has emerged as a promising approach for the repair and regeneration of tissues and organs that are lost, damaged or in general functionally compromised as a result of trauma, injury, disease or aging [1-3]. Calcium metaphosphate (CMP) is a novel scaffold material for tissue engineering. Many studies have demonstrated that calcium metaphosphate ceramics possesses excellent biocompatibility, biodegradability, osteoconductivity and osteoinductivity, and in vivo and in vitro experiments and cell toxicity tests have proven its feasibility as a scaffold material for bone tissue substitutes [4-6].

CMP crystals are relatively stable and degrade slowly [5]. These features are detrimental to the process of new bone formation and thus to tissue engineering scaffold materials. Moreover, high brittleness and easy fatigue failure further prevent the clinical application of CMP. Therefore, we proposed a porous biological ceramic to overcome these disadvantages. Bioactive ceramics can promote bone growth. Active new bone can grow into the interconnected pores of these ceramics to reinforce and

toughen the materials.

Research has shown that [7-13] dense ceramics are not easily degraded in vivo and that the biological activity of these materials can be reduced by their high forming temperatures. In contrast, porous bioceramics promote the circulation of body fluids and the ingrowth of cellular tissue and provide physical support to enable the repair of bone defects. Additionally, stress concentration in pores can enhance stress-induced degradation and increase the surface area of an implant, providing more fracture sites and increasing the susceptibility to wear by environmental factors such as water and oxidation. Pore volume, average pore size and interconnected channel size not only determine the mechanical properties of porous ceramic bone substitutes but also their biological properties. Therefore, these parameters should be precisely controlled to create bone substitute materials with superior performance. Indeed, an increasing number of studies have focused on the development of porous biodegradable ceramics.

Cells can grow into pores larger than 10 μm; 10～20-μm pores allow for the formation of fibrous tissue; 50～100-μm pores enable the formation of bone-like tissue; and pores larger than 150 μm facilitate the formation of mineralized bone [14-16]. If macropores of around 1.0 μm are interconnected, these can promote the assimilation to bone as well as bone formation, [17-21] due to blood circulation and extra-cellular liquid exchange, prior to bone in-growth. Pores with sizes between 1 and 20 μm are important in cellular development, in the type of cells attracted and the orientation and direc-tionality of cellular ingrowth [22]. On the other hand, the interconnected regions of sintered ceramic particles are weakly linked in dissolved ceramics, and these interconnected regions determine the degradability of porous ceramics. As long as the connections are larger than 20 μm, osteoblast ingrowth can occur and cells can be divided in the pores, and connections measuring 20～50 μm can lead to osteoblast ingrowth and promote the growth of cartilage tissue. Therefore, the macro-structure of porous ceramics, especially their porosity, pore size, degree of interconnection and three-dimensional structure, not only affect the mechanical properties of the materials but also have a significant impact on their degradation. The French scholar Lu Jianxi has quantitatively studied the relationship between these connections and the biological effects of these materials, finding that the porous ceramic aperture and the interconnections between holes are extremely important for cell growth, and based on those results, Jianxi suggested an optimal connection length [23].

Although porous bioceramics have many excellent biological properties and have been the subject of

much attention and extensive research in recent decades, many issues remain to be solved to enable their get application [24-27]. For example, (1) Although porous bioceramics is not difficult to obtain high porosity, more research is required to obtain a porous ceramics with a certain pore size distribution, degree of interconnection and three-dimensional structure. (2) The mechanical properties of existing materials are unsatisfactory during the gradual degradation of implants, even if when the materials are completely replaced by new autologous tissue. (3) To improve the structure of porous ceramics，promote cell adhesion, proliferation and migration.

To meet these requirements, various manufacturing methods have been adopted to produce porous ceramics. The structure and properties of porous ceramics are controlled by the preparation process. Porous ceramics obtained by powder sintering and slurry foaming processes have shown closed porous structures. Organic foam impregnation processes have yielded highly porous ceramics with large and fully connected pores. The microporous ceramics with small pore sizes and uniform pore distributions are obtained by sol-gel process.

Porous ceramics prepared by pore-forming agents suffer from the uneven dispersion of pore-forming agents, potentially leading to suboptimal mechanical properties. In addition, the pore-forming and foaming agents are used and other organic matter will have adverse effects on cell growth. Removal of the pore-forming agent may be a considerable problem [28-29]. This paper introduces a novel in situ self-foaming method. The pore-forming process is similar to the method by pore-forming agents using decomposition, gasification and volatilization. In situ self-foaming method does not require an external pore-forming agent. Water vapor is produced by the decomposition of the raw material itself. Because this approach does not suffer from the uneven distribution of pore-forming agents, the pore distribution is absolutely uniform. In addition, this method avoids the production of harmful gases by thermal decomposition of the pore-forming agents, improving the safety of the preparation process.

The purpose of the present study was to explore the application of this method to prepare a porous CMP ceramics scaffolds with uniform and interconnected porosity for tissue engineering purposes and to determine the important variables that control the structural characteristics of the final product. The fabricated samples were characterized by evaluating the development of their pore structure and their mechanical properties.

2. Materials and Methods

2.1 Preparation of monocalcium phosphate monohydrate [$Ca(H_2PO_4)_2.H_2O$ (MCPM)] powder

Monocalcium phosphate monohydrate [$Ca(H_2PO_4)_2.H_2O$ (MCPM)] powders were prepared by chemical precipitation method. Calcium oxide was mixed with phosphoric acid in a Ca/P ratio of 0.5. Reagent-grade calcium oxide (CaO, >98.0%, XiLong Chemical Co., Ltd, China) and phosphoric acid (H_3PO_4, >85.0%, Sinopharm Chemical Reagent Co., Ltd, China) were used as precursors for Ca and P, respectively. Briefly, the reagent-grade H_3PO_4 in amounts of 28.82g were dissolved in 500mL of distilled water to form 0.5 mol/L H_3PO_4 solution. The required amount of 7.01g CaO was slowly added to the above 500 ml of 0.5 mol/L H_3PO_4 solution. The mixed solution was stirred for 48.0 hours in a constant temperature water bath at 30 ℃. The aged solution was dried in an electric thermostatic drying oven for 7 days at 60 ˚C. The dried powders were ground and sieved to 200-mesh for further experiments. The prepared powder is the precursor of MCPM powder.

The theoretical reaction of a powder prepared by isothermal crystallization and chemical precipitation is shown in Eq. (1).

$$CaO + 2H_3PO_4 = Ca\left(H_2PO_4\right)_2 \bullet H_2O \quad (1)$$

2.2 The preparation of monocalcium phosphate anhydrous [$Ca(H_2PO_4)_2$ (MCPA)] and calcium dihydrogen pyrophosphate [$CaH_2P_2O_7$ (CDPP)] powders

Monocalcium phosphate anhydrous [$Ca(H_2PO_4)_2$ (MCPA)] and calcium dihydrogen pyrophosphate [$CaH_2P_2O_7$ (CDPP)] powders were prepared by the heat treatment of MCPM at 140 ˚C for 1.0 hour and at 250 ˚C for 0.5 hour, respectively. Both thermally treated powders were ground and sieved with a 200 mesh.

2.3 The preparation of porous CMP ceramics

The MCPM, MCPA and CDPP powders were individually mixed with 0.5 wt% PVA binder until a uniform mixture was obtained and then each mixture was granulated and sieved. In order to facilitate understanding and memory the porous MCP ceramics were formed by MCPM, MCPA and CDPP powders and are marked as MCPM，MCPA and CDPP ceramics, respectively. These porous ceramic green bodies were formed using uniaxial dry pressing at different pressures with rectangular specimens (powder weight 5g, size is about 60×8×6 mm). The porous ceramics green bodies were formed at the

pressure from 2.0 to 80.0 Mpa, and the specimens were heated at a rate of 0.5 ~3.0 °C /min to 500 °C, respectively. They were subsequently heated to 935 ˚C at the heating rate of 5 ˚C/min for 2.0 hours, and then cooled down to room temperature via natural cooling to yield the porous ceramics samples.

As a comparative experiment with or without the use of a pore-forming agent. A mixture of 10.0% $C_{18}H_{36}O_2$ (SA), a pore-forming agent, with CMP powder (CMP powder is synthesized in our laboratory previously [30]) was milled for 2.0 hours, and 0.5 wt% PVA binder was then added. The mixture was formed at 80 MPa after grinding, granulation and sieved. The green bodies were calcined at 935 ˚C for 2.0 hours with a firing system heating the sample at 5.0 ˚C /min. Porous CMP ceramics were obtained after natural cooling (marked as CMP-SA-10).

2.4 Material analysis

The crystal phases of the synthesized powder and those of the sintered body were examined using a MAC Science MXP^3 X-ray CuKα diffractometer at 40 kV and 20 mA. All micro-FTIR spectra were recorded using the KBr method on an AVATAR 360 Micro-FTIR Jansen Fourier transform infrared spectrometer. Thermal analysis of the powder was performed using a TG-DSC apparatus (DSC 204, Netzsch Co.) at a heating rate of 10 ˚C/min^{-1} from room temperature to 960˚C under air atmosphere. Two powders sample were prepared under each condition in our study for powder analysis. The bending strength of the porous CMP sintered bodies were measured by a three-point bending method in which the supporting parts were set 40 mm apart from one another with a crosshead speed of 0.5 mm/min (CMT-5254 Xinsansi Co.). The porous MCP sintered bodies were used to quantify changes of flexural strength, 6 samples were prepared for flexural strength. The densities of the CMP porous bodies were determined by the water immersion method based on the Archimedean principle. The pore size distribution was measured using mercury intrusion porosimetry (GT-60 of Quantachrome Co.). Scanning electron microscopy (SEM) images were observed with a JEOL JSM-5900 (JSM-5900, JEOL, Tokyo, Japan) scanning electron microscope. All samples were coated with Au before examination by SEM. Three samples were prepared under each condition for density, pore size distribution and the SEM.

3. Results and Discussion

3.1 X-ray diffraction (XRD)

Fig. 1 presents the XRD data obtained for the MCPM powder (CMP precursor) prepared by

isothermal crystallization and chemical precipitation. This powder matched PDF card No. 71-656. The theoretical equation for the powder preparation is presented as Eq. (1).

Fig. 1 also shows the XRD data obtained for the MCPM samples heat treated at 140 ˚C, 250 ˚C and 300 ˚C. The powder heat treated at 140 ˚C for 1.0 hour matched PDF card No. 9-390, $Ca(H_2PO_4)_2$ MCPA, and the sample heated at 250 ˚C for 0.5 hours matched PDF card No. 44-747, $CaH_2P_2O_7$ (CDPP). This data confirmed that MCPA and CDPP powders were obtained at 140 ˚C and 250 ˚C, respectively. The CaO crystal is observed in the three kinds of powders, these are not complete response CaO. In addition, P_2O_5 is observed in the MCPM powders, which is evidence of this acidic precursor. The powder heat treated at 300 ˚C for 2.0 hours was amorphous calcium phosphate (ACP) [30].

3.2 TG-DSC analysis

Fig. 2 presents the TG-DSC profile of MCPM powders heat treated at 140 ˚C and 250 ˚C. MCPM exhibited two endothermic peaks along with mass loss at both 140 ˚C and 250 ˚C, indicating that the decomposition reactions may have occurred at these two temperatures. In addition, an endothermic process between 250 and 450 ˚C was also observed without any distinct endothermic peak. However, TG analysis revealed continuous mass loss in this temperature range, implying an endothermic reaction with slow constant mass loss. A previous study [30, 31] on the evolution of phases with heating of a variety of calcium orthophosphate phases has shown that the acidic phase, $Ca(H_2PO_4)_2.H_2O$ (MCPM), can follow two different decomposition-phase transformation paths.The XRD data discussed above indicate that the MCPM samples heat treated at 140 ˚C and 250 ˚C matched PDF card No. 9-390, $Ca(H_2PO_4)_2$ (MCPA), and PDF card No. 44-747 $CaH_2P_2O_7$ (CDPP), respectively. The MCPM powders heated at 300 ˚C exhibited no distinct characteristic peaks and did not fit any standard PDF card to identify the phase composition. This phase was determined to be similar to an amorphous phase, amorphous calcium phosphate [30]. In conclusion, 1) MCPM is heated to 140℃ to generate MCPA according to Eq. (2), the weight loss of MCPM during this stage is 7.26%. MCPA continues to be heated to 250℃ to generate CDPP according to Eq. (3), the weight loss of MCPA during this stage is 7.22%. Calcium polyphosphate is synthesized according to Eq. (4) or Eq. (5) between 250～450 ˚C. These polycondensation reactions may lead to different crystal spacings. These results are consistent with the XRD data obtained for a continuous amorphous phase spectrum. Overall, these reactions can be described by Eq. (6) for heat-treated MCPM over the temperature range 0～500 ˚C.

The finally calcining temperature of CMP is 935 ºC, purpose is to ensure desired crystalline phase of CMP. CMP melts at around 970 ºC, but at 950 ºC before, CMP is the crystal phase [32]. CDPP was heated between 300-600 ºC, the bond length becomes large. The bond length of CDPP is 0.1622 nm heated between 600-900 ºC, the formation of CMP bond length is 0.1643nm [32, 33], bond length is almost constant duing the high temperature stage. Therefore, abnormal grain growth is minimal.

$$Ca(H_2PO_4)_2 \bullet H_2O \xrightarrow{140^oC} Ca(H_2PO_4)_2 + H_2O \quad (2)$$

$$Ca(H_2PO_4)_2 \xrightarrow{250^oC} CaH_2P_2O_7 + H_2O \quad (3)$$

$$nCaH_2P_2O_7 \xrightarrow{250\sim450^oC} \left[Ca(PO_3)_2\right]_n + nH_2O \quad (4)$$

$$n_1CaH_2P_2O_7 + n_2CaH_2P_2O_7 \xrightarrow{250\sim450℃} \left[Ca(PO_3)_2\right]_{n_1+n_2} + (n_1+n_2)H_2O \quad (5)$$

$$Ca(H_2PO_4)_2 \bullet H_2O \xrightarrow{140^oC} Ca(H_2PO_4)_2 \xrightarrow{260^oC} CaH_2P_2O_7 \xrightarrow{480^oC} Ca(PO_3)_2 \quad (6)$$

3.3 In situ self-foaming properties

The morphologies of the porous CMP ceramics prepared at different molding pressures and heating rates are shown in Fig. 3. MCPM or MCPA powders was molded at 2.0 MPa, or the heating rate at 0.5 ˚C /min (< 500 ˚C) , CMP porous ceramic can be prefabricated with a regular shape at 935 ˚C final calcination temperature, as shown in Fig. 3a-1 and 3b-1. Fig. 3 (c) and (d) present the morphologies of the porous CMP ceramics was used the CDPP and CMP-SA powders, respectively. The two porous CMP ceramics used the CDPP and CMP-SA powders were formed at a pressure 2.0 to 80.0 MPa and the sintered at any heating rate (0.5~10 ˚C/min) without deformation at 935 ˚C final calcination temperature. However, the MCPM and MCPA samples were molded at 40.0 MPa and the sintered at a heating rate of 2.5 ˚C / min (Fig. 3a-2 and 3b-2) were deformed at 935 ˚C final calcination temperature.

3.4 Mechanical properties

Fig. 4 shows the bending strengths of samples molded at different pressures and sintered at different heating rates. These data suggest that MCPM and MCPA molded at any pressure (2.0 to 80 MPa) were not deformed as long as the heating rate remained at 0.5 ˚C/min (under 500 ˚C). In addition, for the MCPM powder, as long as the molding pressure is less than 2MPa, the firing rate in a certain range, it can be formed a rule cuboid. In conclusion, 1) Molding at low pressure (≦2.0 MPa) or sintering at a low

heating rate (≦0.5 ˚C/min) prevented MCPM ceramics deformation. 2) For MCPA ceramics, sintering at a low heating rate (≦0.5 ˚C/min) prevented MCPA ceramics deformation, a heating rate of 1.0 ˚C/min was required to prevent deformation at a molding pressure of 2.0 MPa. 3) CDPP or CMP never deformed at any molding pressure (2.0 to 80 MPa) or heating rate (0.5-10 ˚C/min).

These results could be explained by the fact that each molecule of MCPM lost three water molecules as the temperature increased. This dehydration produced water vapor, and the extent of dehydration of MCPM reached 21.43 wt%, which was the highest level of dehydration among all samples, and MCPM was the densest pore-forming material. When the heating rate was too high, the rapid expansion of water vapor led to deformation in the green bodies. The low heating rate (≦0.5 ˚C/min) resulted in gradual water vapor release, and the low molding pressure (≦2.0 MPa) maintained large gaps in the powder to preserve wide channels facilitating water vapor discharge. The existence of one of these two conditions was sufficient to prevent deformation. Each molecule of MCPA only lost two water molecules, and the level of dehydration of MCPA was 15.38 wt% at high temperature. However, the conditions required to maintain the body shape were much narrower. Only a heating rate below 1.0 ˚C/min and molding at a pressure of 2.0 MPa were able to prevent deformation. This result may be due to deliquescence at ambient temperature, causing the MCPA powder to absorb moisture and to expand, either shrinking or blocking the gas release channels. Rapid heating rates led to the rapid expansion of water vapor, resulting in deformation. Each molecule of CDPP only lost one water molecule at high temperature, and the level of dehydration was only 8.33 wt%. CDPP formed the lowest number of pores. The small amount of water vapor generated at high temperature was not sufficient to cause green body deformation under any conditions (molding pressure 2.0 to 80 MPa or heating rate 0.5-10 ˚C/min).

The average porosity of the samples without deformation was less than 60%. At the same molding pressure, the porous samples sintered at different heating rates without deformation had similar porosities (±2% variation). The porosity of the deformed samples increased with the heating rate. The samples were expanded to a great extent in the middle and less so at the ends, as shown in Figs. 3 (a-2) and (b-2). The ends of the material were less deformed because, whereas the middle portion has four surfaces to discharge gas, the end portion has an extra surface. In general, the samples were more porous at lower molding pressures when the heating rate and the amount of water vapor were held constant. Easier gas discharge limited sample deformation. Accordingly, lower heating rates limited deformation when the molding pressure and gas discharge efficiency were held constant. Taking all of this

information into account, deformation can be prevented in the in situ self-foaming method by adjusting either the molding pressure or the heating rate.

Porosity has a deleterious effect on the properties of ceramic materials, acting as a stress raiser and reducing the mechanical strength [34]. As shown in Fig. 4, the strengths of the samples sintered at different heating rates at the same molding pressure were similar. The strength of the sample molded at 2.0 MPa was only approximately 10.0 MPa, which is far lower than that of the sample molded at high pressure. Higher molding pressures led to stronger porous bioceramics, but excessively high molding pressures caused green body stratification.

At the same heating rate, the effects of molding pressure on strength differed among MCPM, MCPA and CDPP. The strength of MCPM at a heating rate of 0.5 ˚C/min was approximately 30.0 MPa at various molding pressures (above 2.0 MPa). This finding indicates that the molding pressure had little effect on the strength of the sample. MCPA had a slightly higher strength than the other two materials under the same conditions, reaching a maximum of 48.0 MPa among all samples molded at 80.0 MPa and heated at 0.5 ˚C/min. The strength of CDPP first increased with molding pressure and then exhibited no effect. The maximum strength for both MCPM and CDPP occurred at approximately 30.0 MPa and was only 60% of the strength of MCPA.

3.5 Porosity and pore size distribution

The porosities of MCPM, MCPA and CDPP ceramics prepared at different molding pressures and different heating rates are shown in Fig. 5. The porosity increased gradually with increasing heating rate and decreasing molding pressure as shown in Figs. 5(A) and (B). The porosity was not affected by changes in the heating rate, as observed in Fig. 5(C).

Fig. 6 presents the pore size distributions of MCPM, MCPA, CDPP and CMP-SA-10 ceramics created at a molding pressure of 80 MPa and sintered at 935 ˚C for 2.0 hours at a heating rate of 0.5 ˚C/ min below 500 ˚C. These data suggest that the pore size distributions of MCPM-0.5-2 (0.5: heating rate at 0.5 ˚C/ min, 2: calcination holding time 2.0 hours, follow is the same.), MCPA-0.5-2, CDPP-0.5-2 and CMP-SA-10 ceramics were Gaussian-distributed and similar among the materials. The aperture was close to the average pore diameter. The pore diameters (distribution range) of MCPM, MCPA, CDPP and CMP-SA -10 ceramics were 32.78 μm (10～60 μm), 18.89 μm (10～22 μm), 3.603 μm (0.7～7.0 μm) and 2.907 μm (0.4～6 μm), respectively. Potoczek et al. produced HA and calcium phosphate foams

with pore size in the range 130–380 mm and 350-900 mm, respectively [35,36]. Ramay and coworkers obtained HA foams with the pore size in the range 200-400 mm [37]. Since, minimum pore size required to enable ingrowth of surrounding bone with blood supply is about 1.0–20 mm [22] and with larger pores the strength of the foams decreases significantly [38], obtaining the minimum pore size capable of filling with surrounding bones is very important.

These pores (10～60 μm) for MCPM and MCPA ceramics result in the formation of bone-like and fibrous tissue [14-16]. The pores (0.7～7.0 μm) for CDPP ceramics are important in cellular development, because they can promote the assimilation to bone as well as bone formation, promote the type of cells attracted and orientation and directionality of cellular ingrowth [17-22]. CDPP ceramics exhibited the widest pore size distribution, while MCPM showed the narrowest distribution. The pore size distribution appeared as a single peak for CDPP, implying that the green body had a smaller pore size. These data further confirm that the pores in MCPM, MCPA and CDPP resulted from the release of water vapor, making this fabrication process similar to that driven by pore-forming agents. CDPP powders showed a lower water content than the other powders, and its weight loss occurred slowly and constantly as the temperature increased from 250 ˚C to 450 ˚C, indicating slow and constant water vapor release. The water vapor built up at low pressure, resulting in a small pore size and a widest wider size distribution in CDPP. In contrast, MCPA released water vapor gas by two different processes, described by Eqs. (3) and (4). The process represented by Eq. (3) occurred at 250 ˚C, and water vapor was released dramatically at high pressure. The high water vapor pressure created larger pores with a wider size distribution. MCPM also exhibited an additional water vapor release process, described by Eq. (2). The additional water vapor release described by Eq. (2) increased the pore size and narrowed the pore size distribution of MCPM. Comparing the pore size distributions among these three materials revealed that MCPA and MCPM ceramics were similar to one another and distinct from CDPP. The process described by Eq. (2) is regarded to be responsible for creating the 22～60 μm pores in MCPM, and the process described by Eq. (2) or (3) or both is believed to be responsible for the formation of the 10～22 μm pores. The extents of the three reactions affected the pore size and its distribution followed the order Eq. 2>Eq. 3>Eq. 4. This finding provides suitable guidelines on which future efforts can be based to produce porous MCP ceramics with a particular pore size and pore size distribution.

As a comparison group of CMP-SA-10，wich exhibited more narrow pore size distribution than CDPP, also a single hole. This is because the pore-forming agent is single.

3.6 Scanning electron microscopy (SEM)

Fig. 7 presents SEM micrographs of MCPM-0.5-1, MCPA-0.5-1, CDPP-0.5-1 and CMP-SA-10. The apertures observed in these images are consistent with the measurements made by the mercury intrusion method. The grain size was approximately 5-10 μm. The aperture was homogeneous across MCPM, MCPA and CDPP, whereas the pore size distribution tended to narrow. Among these three materials, the sample in Fig. 7C show the highest degree of interconnection, which promotes body fluid circulation, cellular adhesion and the ingrowth of cellular tissue [14-22] . As can be seen in Fig. 7b, this leads to the formation of a network of open pores [37].

This result suggests that this material would be the most suitable for bone tissue engineering applications.

Fig. 7D is the SEM micrograph of a comparative experiment with the use of a pore-forming agent. The porous ceramics of CMP-SA-10 prepared by pore-forming agents suffer from the uneven dispersion of pore-forming agents.

3.7 Relationship between porosity and strength

Fig. 8 plots the porosity versus the strength of MCPM, MCPA, CDPP and CMP-SA. The strengths of these materials were compared at the same porosity and were determined to follow the order MCPA > MCPM > CDPP > CMP-SA. The strengths of MCPM is lower than MCPA, possibly because MCPM possessed a high water content. The water vapor was released in a violent process via Eq. (2). The high water vapor pressure produced larger pores on average with a broader distribution, leading to many MCPM defects. The strength enhancement was overshadowed by these negative factors. The formation processes of MCPA does not involve the reaction described by Eq. (2). The small apertures and narrow pore size distributions in this materials further enhanced their strength. In contrast, the bending strength of CDPP was worse than that of MCPM, which may be attributed to the fact that CDPP contains less water, easy to melt. The melted CPP is capable of merging many grains together to form a gas-proof supergrain that would defy the emission of the water gas [38]. Thus, sphere pores were generated and bending strength decreased and their size increased.

In these samples, the flexural strength of the control group CMP-SA is lowest. As shown in fig. 7, the grain sizes of MCPM, MCPA and CDPP to CMP-SA indicated that they were all in the range of 5.0～20.0 μm. However, CMP-SA clearly exhibited the broadest grain size distribution. This may be due to

the role of pore-forming agent, it makes the microstructure of the materials distribution is not uniform, forming a continuous series of pores like cracks. From the result, the defects of pore-forming agent in the synthesis of porous body is very obvious.

4. Conclusions

Porous ceramics were synthesized using an in situ self-foaming method, and the preparation process and the properties of resulting material were studied. MCPM and MCPA powders molded at low pressure (≦2.0 MPa) or sintered at a low heating rate (≦0.5 ˚C/min) as well as CDPP powder heat treated at 250 ˚C can be fabricated into porous biomaterials without pore-forming agents. The other powders or conditions tested exhibited various degrees of deformation. The porous CMP biological ceramics produced by MCPA powders at 80 MPa and a heating rate of 0.5 ˚C/min exhibited 38.0% porosity and a strength of 40.0 MPa. Compared to the pore-forming agent method, this in situ self-foaming method can generate materials with a small grain size, a narrow grain size distribution, a larger specific surface area and a higher breaking strength. This method can overcome the shortcomings of the pore-forming agent method, principally the uneven distribution of pore-forming agents, which leads to an uneven pore distribution and poor porosity control and thus a decrease in strength. This approach could be applied to fabricate many other porous materials for a variety of applications.

Acknowledgment

This project was funded by the Priority Academic Program Development of Jiangsu Higher Education Institutions and “12th Five-Year Plan” to support science and technology key project (No.2011BAE30B01).

References

[1] Nerem RM. Cellular engineering, Ann. Biomed. Eng. 19 (1991) 529-545.

[2] Langer R, Vacanti JP. Tissue engineering, Science. 260 (1993) 920-926.

[3] Chiara R, Alessandra G, Serena M, Francesco B, Emanuel L, Francesco B, Chiara VB. Microstructural characterization and *in vitro* bioactivity of porous glass-ceramic scaffolds for bone regeneration by synchrotron radiation X-ray microtomography. J. Eur. Ceram. Soc. 33 (2013) 1553-1565.

[4] Park EK, Lee YE, Choi JY, Oh SH, Shin HI, Kim KH, Kim SY, Kim Sk. Cellular biocompatibility and stimulatory effects of calcium metaphosphate on osteoblastic differentiation of human bone marrow-derived stromal cells, Biomaterials. 25 (2004) 3403-3411.

[5] Lee YM, Seol YJ, Lim YT, Kim S, Han SB, Rhyu IC, Baek SH, Heo SJ, Choi JY, Klokkevold PR, Chung CP. Tissue‐engineered growth of bone by marrow cell transplantation using porous calcium metaphosphate matrices, J. Biomed. Mater. Res. 54 (2001) 216-223.

[6] Fujiu T, Messing GL, Huebner W. Processing and Properties of Cellular Silica Synthesized by Foaming Sol‐Gels, J. Am. Ceram. Soc. 73 (1990) 85-90.

[7] Yang YF, Zhao YH, Tang GW, Li H, Yuan XY, Fan YB. < i> In vitro</i> degradation of porous poly (l-lactide-< i> co</i>-glycolide)/β-tricalcium phosphate (PLGA/β-TCP) scaffolds under dynamic and static conditions, Polym. Degrad. Stabil. 93 (2008) 1838-1845.

[8] Correa J, Domínguez VM, Martínez M, Vidal G. Aerobic degradation of 2, 4, 6-TCP content in ECF bleached effluent, Environ. Int. 29 (2003) 459-465.

[9] Jin HH, Min SH, Song YK, Park HC, Yoon SY. Degradation behavior of poly (lactide-co-glycolide)/β-TCP composites prepared using microwave energy, Polym. Degrad. Stabil. 95 (2010) 1856-1861.

[10] Cáceres TY, He WX, Naidu RV, Megharaj MV. Toxicity of chlorpyrifos and TCP alone and in combination to< i> Daphnia carinata</i>: The influence of microbial degradation in natural water, Water. Res. 41 (2007) 4497-4503.

[11] Wang J, Li CW, Luan XY, Li J, Wang BX, Zhang LQ, Xu R, Zhang XD. Investigation on solar photocatalytic activity of TiO2 loaded composite: TiO2/Skeleton, TiO2/Dens and TiO2/HAP. J. Mol. Catal. A-Chem. 320 (2010) 62-67.

[12] Veljović D, Jokić B, Petrović R, Palcevskis Dindun E, A, Mihailescu IN, Janac kD. Processing of dense nanostructured HAP ceramics by sintering and hot pressing, Ceram. Int. 35 (2009) 1407-1413.

[13] Ignjatović N, Savić V, Najman S, Plavsic M, Uskokovic D. A study of HAp/PLLA composite as a substitute for bone powder, using FT-IR spectroscopy, Biomaterials. 22 (2001) 571-575.

[14] Bitou M, Okamoto M. Fabrication of porous 3-D structure from poly (l-lactide)-based nano-composite foams. Effect of foam structure on enzymatic degradation, Polym. Degrad. Stabil. 93 (2008) 1081-1807.

[15] Oh SH, Park IK, Kim JM, Lee JH. In vitro and in vivo characteristics of PCL scaffolds with pore size gradient fabricated by a centrifugation method, Biomaterials. 28 (2007) 1664-1671.

[16] Tienen TGV, Heijkants RGJC, Buma P, Groot JHD, Pennings AJ, Veth RPH. Tissue ingrowth and degradation of two biodegradable porous polymers with different porosities and pore sizes, Biomaterials. 23 (2002) 1731-1738.

[17] Engin NO, Tas AC. Manufacture of macroporous calcium hydroxyapatite bioceramics, J. Euro. Ceram. Soc. 19 (1999) 2569-2572.

[18] Passuti N, G Daculsi, Rogez JM, Martin S, Bainvel JV. Macroporous calcium phosphate ceramic performance in human spine fusion, Clin.Orthoped., 148, (1989)169-176.

[19] Hu J, Russel JJ, Ben-Nissan B, Vago R. Production and analysis of hydroxyapatite from Australian corals via hydrothermal process, J. Mater. Sci. Lett. 20 (2001) 85-87.

[20] Zhang Y, Yokogawa Y, Kameyama T. Preparation of Bimodal Porous Apatite Ceramics Through Slip Casting Using Fine Hydroxyapatite Powders, Key. Eng. Mater. 317 (2006) 723-728.

[21] Zhang Y, Deshuang K, Yokogawa Y, Xia F., Tao YQ, Tai Q. Fabrication of Porous Hydroxyapatite Ceramic Scaffolds with High Flexural Strength Through the Double Slip‐Casting Method Using Fine Powders, J. Am. Ceram. Soc. 95 (2012) 147-152.

[22] S´anchez-Salcedo S, Nieto A, Vallet-Reg´M. Hydroxyapatite/β-tricalcium phosphate/agarose macroporous scaffolds for bone tissue engineering, Chem. Eng. J. 137 (2008) 62-71.

[23] Lu JX, Flautre B, Anselme K. Study of porous interconnections of bioceramic on cellular rehabilitation in vitro and in vivo, Bioceramics. 10 (1997) 583-586.

[24] Agrawal CM, Athanasiou KA, Heckma JD. Biodegradable PLA-PGA polymers for tissue engineering in orthopaedics, Mater. Sci. Forum. 205 (1997) 115-128.

[25] Cima LG, Vacanti JP, Vacanti C, Ingber D, Mooney D, Langer R. Tissue engineering by cell transplantation using degradable polymer substrates, J. Biomech. Eng. 113 (1991) 143-151.

[26] Agrawal CM, Athanasiou KA. Technique to control pH in vicinity of biodegrading PLA-PGA implants, J.

Biomed. Mater. Res. 38 (1997) 105-114.

[27] Hsu FY, Chueh SC, Wang Y. Microspheres of hydroxyapatite/reconstituted collagen as supports for osteoblast cell growth. J. Biomaterials. 20 (1999) 1931-1936.

[28] Koh YH, Lee EJ, Yoon BH, Song J H, Kim HE. Effect of Polystyrene Addition on Freeze Casting of Ceramic/Camphene Slurry for Ultra‐High Porosity Ceramics with Aligned Pore Channels, J. Am. Ceram. Soc. 89 (2006) 3646-3653.

[29] Han JC, Hong CQ, Zhang XH, Du JC, Zhang W. Highly porous ZrO< sub> 2</sub> ceramics fabricated by a camphene-based freeze-casting route: Microstructure and properties, J. Eur. Ceram. Soc. 30 (2010) 53-60.

[30] TenHuisen KS, Brown PW. Phase Evolution during the Formation of α‐Tricalcium Phosphate, J. Am. Ceram. Soc., 82 (1999) 2813–2818.

[31] McIntosh AO, Jablonski WL. X-ray diffraction powder patterns of calcium phosphates, Anal. Chem. 28 (1956) 1424–1427.

[32] Liang Xiao-Feng, Yang Shi-Yuan and Yin Guang-Fu. Raman Spectra Analysis for Calcium Metaphosphate Structure Transformation in Glass Preparation Process. Chinese Journal of Inorrganic Chemistry. 8 (2010) 1404-1408.

[33] L. Popovic´, D. de Waal and J. C. A. Boeyens. Correlation between Raman wavenumbers and P-O bond lengths in crystalline inorganic phosphates. J. Raman Spectrosc., 2005,36:2-11.

[34] Alves HLR, Dos Santos LA, Bergmann CP. Injectability evaluation of tricalcium phosphate bone cement, J. Mater. Sci.: Mater. Med. 19 (2008) 2241-2246.

[35] Potoczek M. Hydroxyapatite foams produced by gelcasting using agarose, Mater. Lett. 62 (2008) 1055–1057.

[36] Potoczek M, Zima A, Paszkiewicz Z, Slosarczyk A. Manufacturing of highly porous calcium phosphate bioceramics via gel-casting using agarose, Ceram. Int. 35 (2009) 2249–2254.

[37] Ramay HR, Zhang M. Preparation of porous hydroxyapatite scaffolds by combination of the gel-casting and polymer sponge methods, Biomaterials. 24 (2003) 3293–3302.

[38] Sopyan I, Mel M, Ramesh S, Khalid KA. Porous hydroxyapatite for artificial bone applications, Sci. Technol. Adv. Mater. 8 (2007) 116–123.

[37] Deville S, Saiz E, Tomsia AP. Freeze casting of hydroxyapatite scaffolds for bone tissue engineering, Biomaterials 27 (2006) 5480–5489.

[38] Omelon S, Baer A, Coyle T, Pilliar RM, Kandel R, Grynpa M. Polymeric Crystallization and Condensation of Calcium Polyphosphate Glass, Mater. Res. Bull. 43 (2008) 68-80.

List of Figures

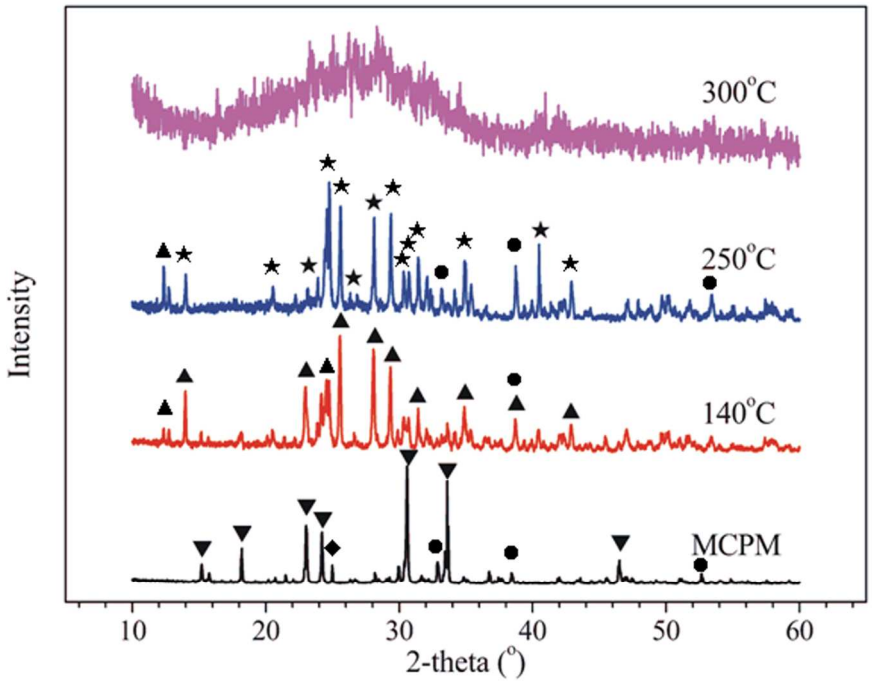

Fig. 1. The XRD patterns of the MCPM precursor powder synthesized by the isothermal crystallization chemical precipitation method and of MCPM heated at 140 oC, 250 oC and 300 oC, Labels are as follows: ▼(MCPM), ▲ (MCPA), ★ (CDPP), ● (CaO), ◆ (P2O5).
165x117mm (300 x 300 DPI)

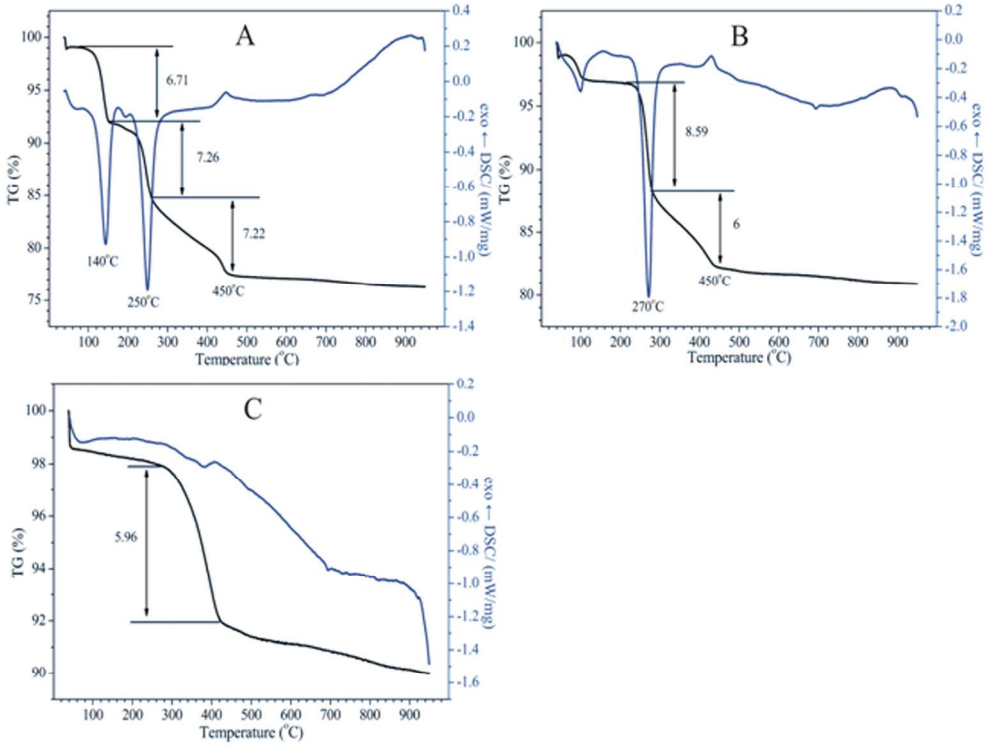

Fig. 2. The TG-DSC profile of the MCPM powder without heat treatment (A), after heat treatment at 140 °C (B) and 250 °C (C).
179x139mm (300 x 300 DPI)

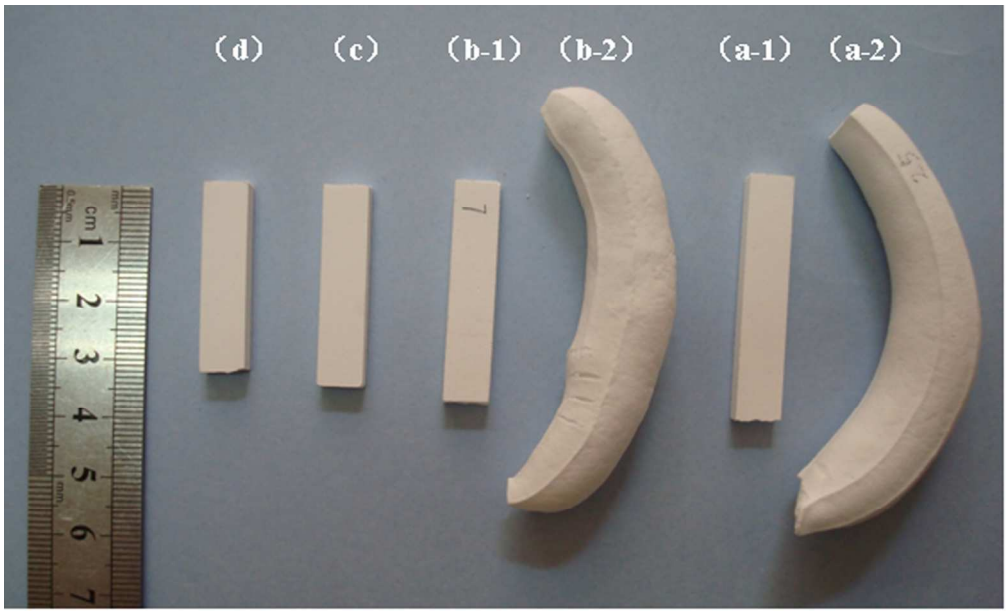

Fig. 3. The morphology of the samples formed at different molding pressures or sintered at different heating rates: (a-1) (a-2) MCPM powder molded at 2.0 and 40.0 MPa, respectively. (b-1) (b-2) MCPA powder sintered at 0.5 (under 500 °C) and 2.5 °C/ min, respectively. (C) CDPP powder and (d) CMP-SA powder formed at any pressure or any heating rate.
125x76mm (300 x 300 DPI)

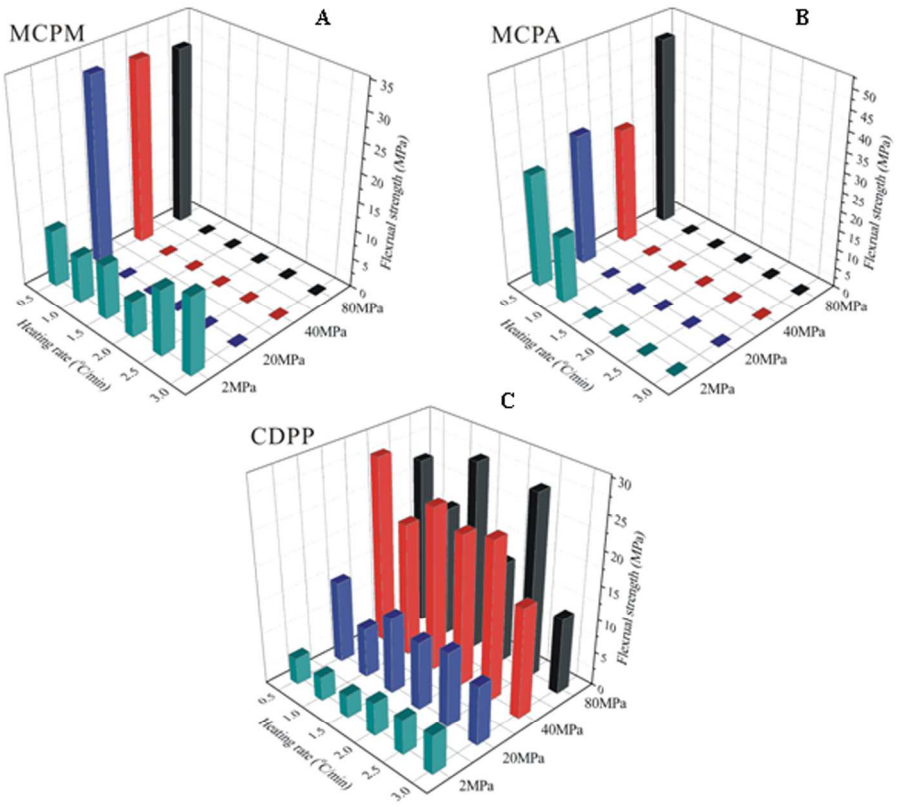

Fig. 4. The bending strengths of the sintered samples molded at different pressures and sintered at different heating rates: (A) MCPM, (B) MCPA and (C) CDPP.
191x159mm (300 x 300 DPI)

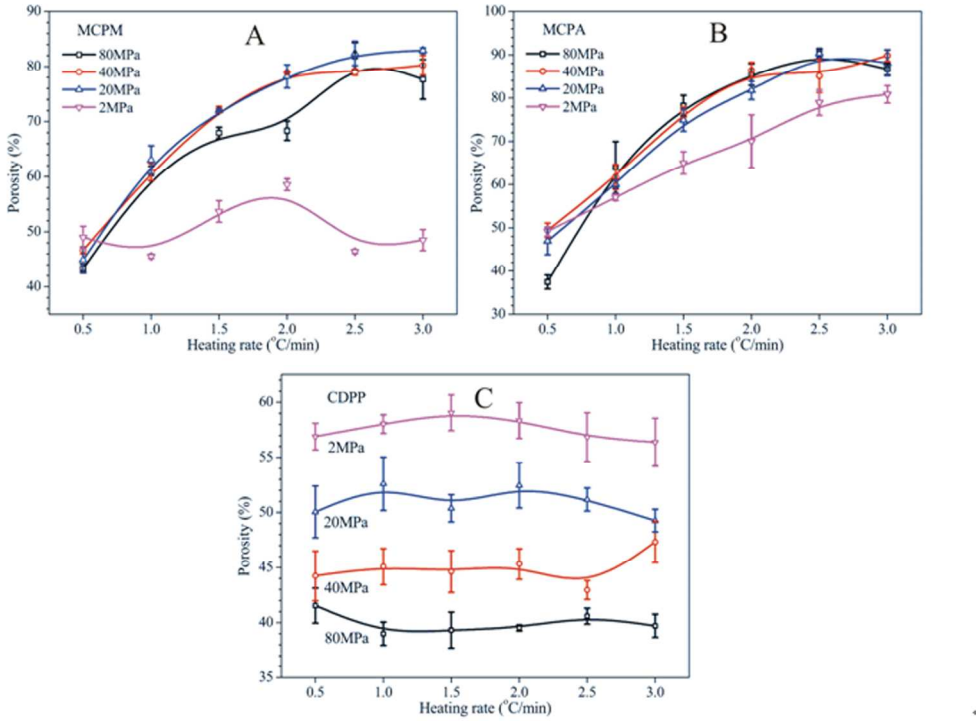

Fig. 5. The porosities of the samples formed at different molding pressures and sintered at different heating rates: (A) MCPM, (B) MCPA and (C) CDPP.
192x150mm (300 x 300 DPI)

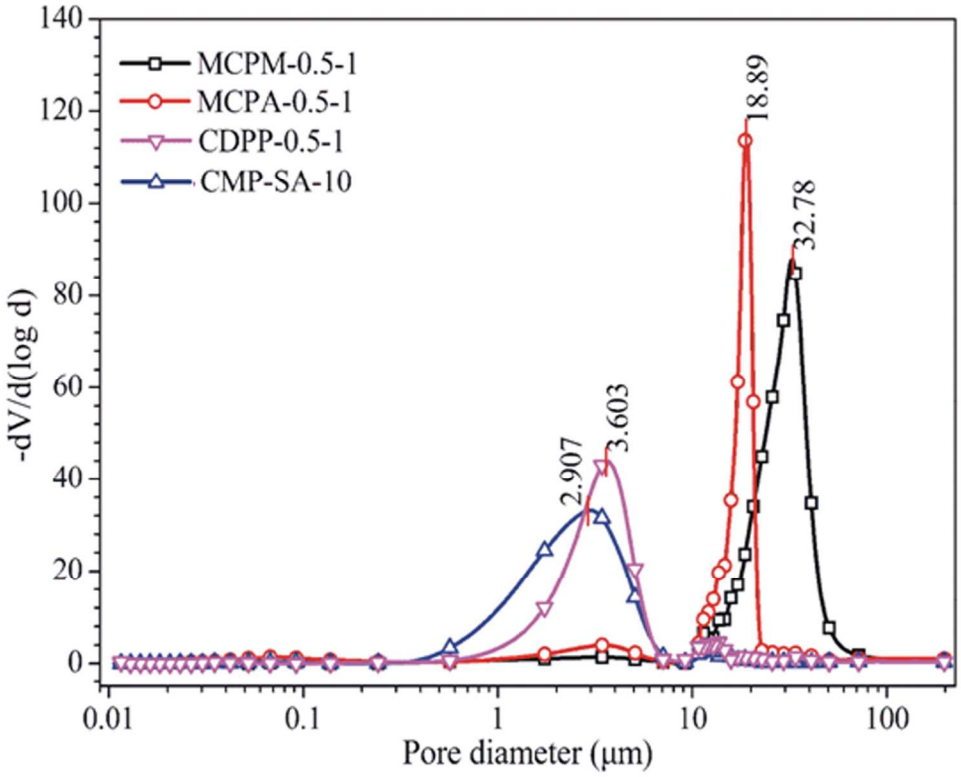

Fig. 6. The pore size distribution of samples (CMP-SA-10, MCPM, MCPA and CDPP) molded at 80.0 MPa and sintered at 935 °C for 2.0 hours at a heating rate of 0.5 °C/min below 500 °C.
201x160mm (300 x 300 DPI)

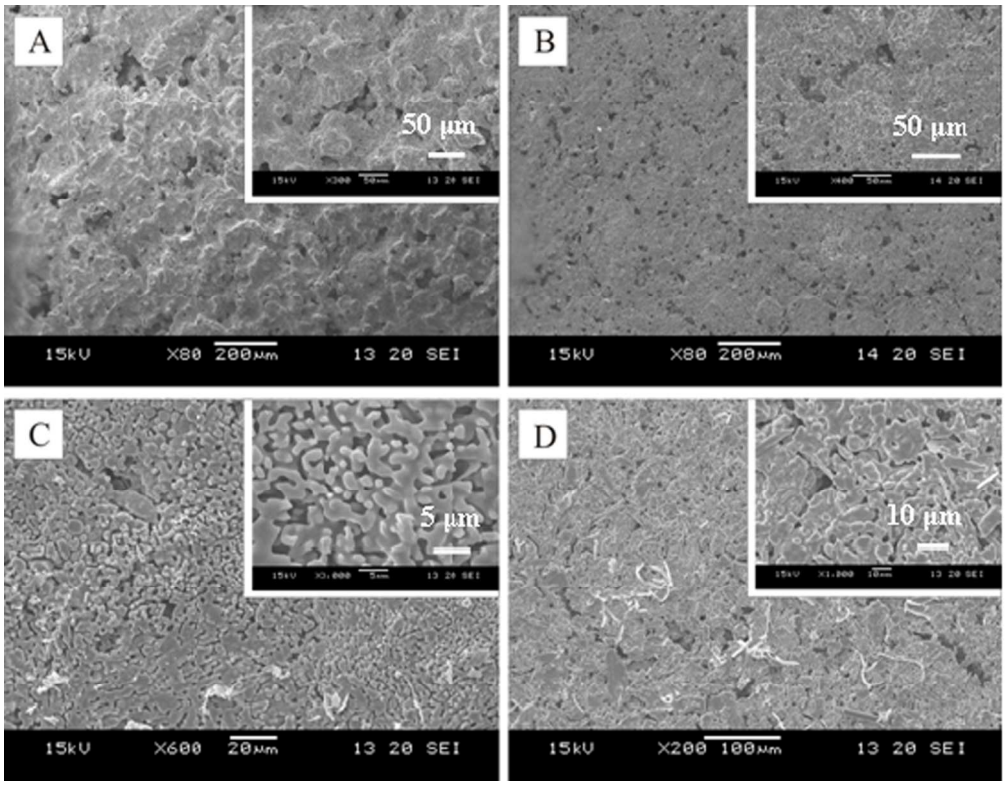

Fig. 7. SEM micrographs of (A) MCPM-0.5-1, (B) MCPA-0.5-1, (C) CDPP-0.5-1 and (D) CMP-SA-10.
148x115mm (300 x 300 DPI)

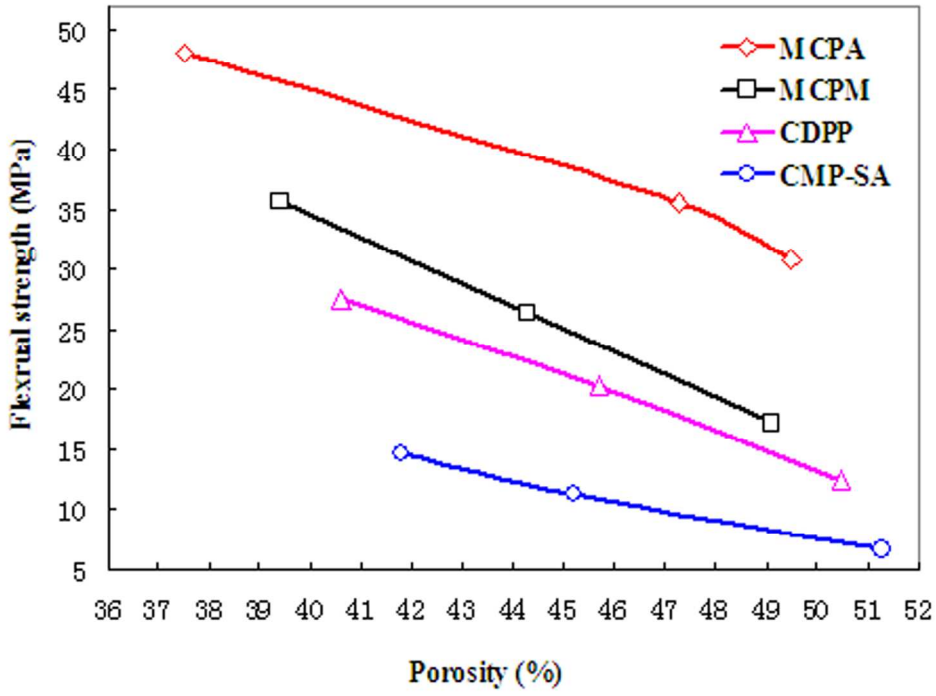

Fig. 8. The relationship between porosity and strength for the porous bodies of MCPM, MCPA, CDPP and CMP-SA.
167x126mm (300 x 300 DPI)